

# Beyond Degradation Conditions: All-in-One Image Restoration via HOG Transformers

Jiawei Wu<sup>1</sup>, Zhifei Yang<sup>2</sup>, Zhe Wang<sup>1</sup>, Zhi Jin<sup>1,3,\*</sup>

<sup>1</sup> School of Intelligent Systems Engineering, Shenzhen Campus of Sun Yat-sen University, Guangdong, China

<sup>2</sup> School of Computer Science, Peking University, China

<sup>3</sup> Guangdong Provincial Key Laboratory of Fire Science and Technology, Guangzhou, China

wujw97@mail2.sysu.edu.cn

## Abstract

All-in-one image restoration, which aims to address diverse degradations within a unified framework, is critical for practical applications. However, existing methods rely on predicting and integrating degradation conditions, which can misactivate degradation-specific features in complex scenarios, limiting their restoration performance. To address this issue, we propose a novel all-in-one image restoration framework guided by Histograms of Oriented Gradients (HOG), named HOGformer. By leveraging the degradation-discriminative capability of HOG descriptors, HOGformer employs a dynamic self-attention mechanism that adaptively attends to long-range spatial dependencies based on degradation-aware HOG cues. To enhance the degradation sensitivity of attention inputs, we design a HOG-guided local dynamic-range convolution module that captures long-range degradation similarities while maintaining awareness of global structural information. Furthermore, we propose a dynamic interaction feed-forward module, efficiently increasing the model capacity to adapt to different degradations through channel-spatial interactions. Extensive experiments across diverse benchmarks, including adverse weather and natural degradations, demonstrate that HOGformer achieves state-of-the-art performance and generalizes effectively to complex real-world degradations. Code is available at <https://github.com/Fire-friend/HOGformer>.

## CCS Concepts

• **Computing methodologies** → **Computer vision**.

## Keywords

All-in-one image restoration, Dynamic self-attention, Histogram of oriented gradients (HOG), Transformer

## 1 Introduction

Real-world images often suffer from diverse degradations, including blur, low illumination, and adverse weather conditions. While recent deep learning advances have significantly improved image restoration for specific degradations [15, 16, 50, 58, 70], these approaches typically require separate models for each degradation, increasing computational costs and deployment complexity. To address this issue, all-in-one image restoration [18] has emerged as a more challenging yet practical solution, unifying various degradation handling within a unified model. This capability is particularly crucial for real-world applications like autonomous driving [6], where input conditions are highly dynamic and unpredictable.

The computer vision community has witnessed growing interest in all-in-one image restoration [2, 21, 24, 48, 55, 66, 69]. The pioneering approach [27] employs separate encoders for different

degradations, necessitating independent training procedures and compromising scalability. Recent advances [2, 21, 24, 48] improve upon these limitations through degradation-related conditioning mechanisms, where degradation features are extracted and injected into a shared network backbone to enable dynamic adaptation. However, the insufficient extraction and merging of conditional features often result in feature conflicts that can compromise the quality of restoration, especially when dealing with complex degradation scenarios. Parallel efforts [1, 69] explore Mixture-of-Experts (MoE) frameworks, which assemble specialized restoration sub-networks with adaptive routing mechanisms. Although MoE architectures offer greater flexibility, they inherently incur significant computational costs and scalability limitations. Despite advancements in conditioning mechanisms and MoE paradigms, current methods have practical limitations, such as insufficient generalization to unseen degradations and excessive resource consumption.

In this work, we observe that the Histogram of Oriented Gradients (HOG) feature descriptor [12] inherently characterizes and distinguishes different degradations. As shown in Figure 1, HOG features effectively identify both natural and adverse weather (Figure 1(b)) degradations. The descriptive power of HOG arises from its core components, gradient magnitude and orientation, which jointly encode local intensity and directional structure. These gradient properties offer discriminative cues that are sensitive to degradation-specific patterns. For instance, in the case of rain degradation (Figure 1(a)), rainfall generates vertical streaks that manifest as prominent vertical gradients, whereas raindrop regions appear as circular isolated patches with low gradient magnitudes. In contrast, snow results in widespread high-magnitude gradients with minimal directional bias, producing dense and uniform textures. These phenomena suggest that each degradation exerts unique and quantifiable effects in the gradient domain. Hence, this observation motivates a natural question: *Can the ability of HOG to capture local intensity and directional structures be effectively used to design a more efficient all-in-one image restoration network?*

To this end, we propose a novel Histogram of Oriented Gradients Transformer, called HOGformer, for all-in-one image restoration. The core innovation is a Dynamic HOG-aware Self-Attention (DHOCSA) mechanism that reformulates standard self-attention by incorporating HOG descriptors, significantly enhancing restoration performance across diverse degradations. DHOCSA integrates patch-level and pixel-level HOG descriptors, adaptively emphasizing spatial regions based on perceptual degradation. This attention mechanism prioritizes critical gradient orientations and magnitudes, enabling more robust feature representation for all-in-one

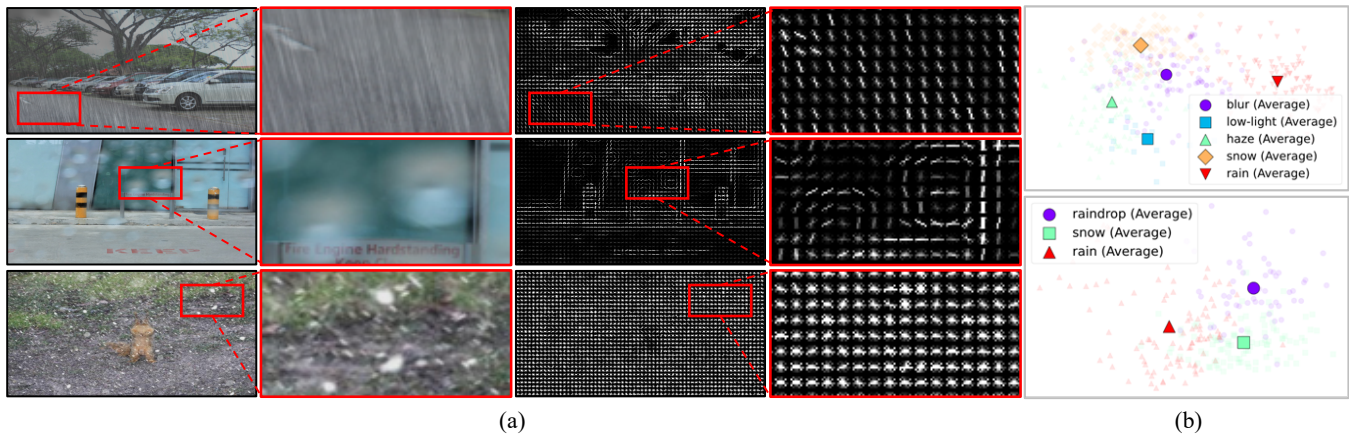


**Figure 1: Visualization of HOG feature distributions under various degradations. (a) Example images of different weather conditions with corresponding HOG feature visualizations. (b) HOG features for five natural degradations [79] and three adverse weather degradations [55], using 100 randomly selected images for each degradation.**

restoration. To capture degradation-related dependencies and enable efficient feature extraction in this attention mechanism, we propose a local dynamic-range convolution using pixel-level HOG descriptors, along with two HOG reshaping methods: bin-wise HOG reshaping (BHOGR) for global context and frequency-wise HOG reshaping (FHOGR) for local detail preservation. Besides, to make the feed-forward module in the transformer capable of adapting to various degradations, we propose an efficient Dynamic Interaction Feed-Forward (DIFF) module, which promotes global information exchange through shuffle and gated mechanisms across spatial and channel dimensions. Moreover, we propose a HOG loss that supervises gradient orientation and magnitude to preserve edge and structural integrity. These components enable HOGformer to effectively restore various degraded images in a unified model, achieving state-of-the-art performance in both adverse weather and natural image restoration tasks.

The primary contributions of this work are as follows:

- We propose a novel all-in-one image restoration method called HOGformer, which utilizes the discriminative power of HOG features to address various image degradations.
- We introduce a dynamic HOG-aware self-attention mechanism that incorporates gradient orientations and magnitudes at both patch and pixel levels. This mechanism adaptively emphasizes spatial regions based on perceptive degradations. Additionally, we propose a local dynamic-range convolution to capture degradation-related dependencies, which further enhances the attention input.
- We design innovative network components, including a dynamic interaction feed-forward module to address diverse degradations through channel-spatial information exchange, and HOG loss to preserve edge and structural integrity.

## 2 Related Works

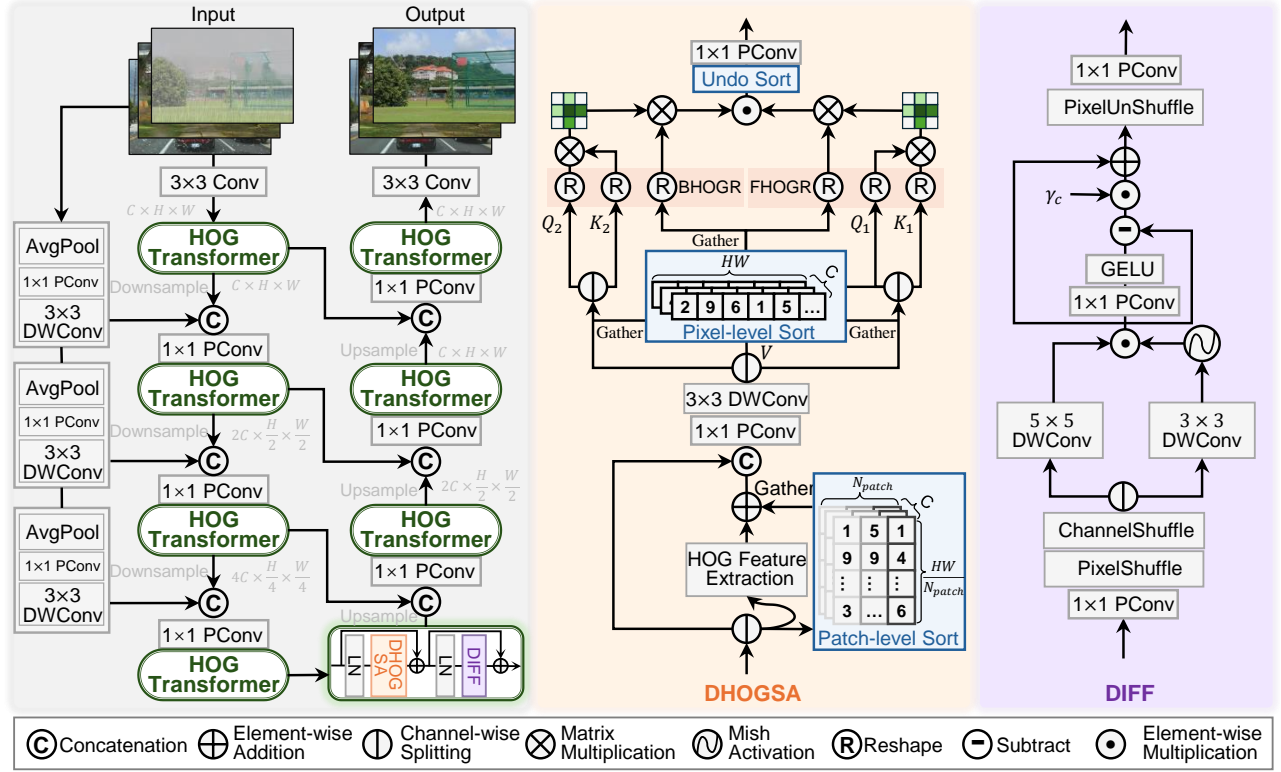
### 2.1 Single-Task Image Restoration

Image restoration is a fundamental task in computer vision. To obtain well-defined results, methods frequently integrate human

knowledge, prior information, and handcrafted features to constrain the solution space [3]. In recent years, with the development of deep learning, many methods [15, 16, 50, 58, 70] have been proposed and achieved outstanding performance in image restoration tasks. The introduction of the Vision Transformer has notably enhanced performance by modeling long-range dependencies [31, 31, 63, 70]. For example, Swin-IR [31] employs the Swin Transformer [36] for image restoration, using its shifted window mechanism to enhance local and global contextual understanding. Restormer [70] incorporates an efficient multi-stage design with attention mechanisms to address degradation while maintaining computational efficiency. Transformer-based methods have recently been developed for tasks such as deraining [10], desnowing [7], dehazing [54, 78], deblurring [22, 32], and low-light enhancement [4, 77]. Although task-specific models have shown satisfactory results, they lack generalization capabilities when faced with degradation beyond specific ones [55]. These methods require training models separately for different datasets and tasks, consuming a lot of resources. This impedes their deployment in practical applications.

### 2.2 All-in-One Image Restoration

All-in-one image restoration [18, 24, 55, 79] uses a single model to address various degradation tasks without task-specific retraining, which significantly improves efficiency and usage. However, there are still limitations in all-in-one image restoration frameworks. InstructIR [11] specifies restoration targets through natural language instructions, but requires high data preparation costs. Painter [62], DA-CLIP [40] utilize on-the-fly learning to unleash the potential of large models. DiffUIR [79] achieves multi-degradation restoration based on the residual diffusion model [34]. PromptIR [48] uses prompts to encode degraded specific information and dynamically guide network recovery. These methods are all based on specific conditions constructed according to different degradation, in order to endow the network with a flexible feedforward process to handle different degradations. However, the construction of these degradation-related conditions is relatively complex and lacks a



**Figure 2: The overall architecture of our HOGformer. It includes the HOG Transformer block with the Dynamic HOG-aware Self-Attention (DHOOGSA) module and Dynamic Interaction Feed-Forward (DIFF) module.**

guaranteed framework or prior knowledge to ensure their effectiveness. Recently, Histoformer [55] introduces prior knowledge of grayscale histograms into Transformer and achieves excellent results in adverse weather image restoration tasks. However, histograms cannot distinguish all degradation well, for example, the difference between the histogram of a blurry image and a normal image is very small. Unlike these methods, we incorporate the core concept of HOG features into our all-in-one image restoration model. This allows us to effectively utilize HOG features to differentiate between various types of degradation and effectively achieve all-in-one image restoration.

### 3 Method

#### 3.1 Overall Architecture

Figure 2 illustrates the overall architecture of HOGformer. Given a low-quality input image  $I^lq \in \mathbb{R}^{3 \times H \times W}$ , a  $3 \times 3$  convolution is first applied to embed overlapping patches. The encoder and decoder are composed of HOG Transformer Blocks (HOGTBs), which extract complex features and model dynamic degradation patterns. Within each stage, skip connections link the encoder and decoder to preserve intermediate features and stabilize the training process. Between stages, pixel-unshuffle and pixel-shuffle operations are used for downsampling and upsampling, respectively.

The key component of our HOGformer, i.e., HOGTB, consists of two proposed modules: Dynamic HOG-aware Self-Attention

(DHOOGSA) and Dynamic Interaction Feed-Forward (DIFF). These components interact with layer normalization in the following way:

$$\begin{aligned} F_l &= F_{l-1} + \text{DHOOGSA}(\text{LN}(F_{l-1})), \\ F_l &= F_l + \text{DIFF}(\text{LN}(F_l)), \end{aligned} \quad (1)$$

where  $F_l$  and  $\text{LN}$  denote the feature at  $l_{th}$  stage and layer normalization, respectively. DHOOGSA dynamically focuses on spatial range based on perceived degradation and facilitates both local and global feature aggregation by two bin allocation mechanisms, while DIFF improves the capacity of model to handle various degradations. During each stage of the encoder, a coarse skip connection supplements the original input features through a sequence of operations, including average pooling, pointwise convolution, and deep convolution [55]. Coarse skip connections are applied from the second stage onward, enabling the encoder to focus more effectively on learning degradation-induced residuals. This hybrid design leverages the ability to distinguish degraded priors based on gradient orientation and magnitude, allowing HOGformer to adapt to various degradations.

#### 3.2 Dynamic HOG-aware Self-Attention

To model the dynamic distribution of degradations with respect to both gradient orientation and magnitude, we propose a Dynamic Histogram of Oriented Gradients Self-Attention (DHOOGSA) module. DHOOGSA includes a local dynamic-range convolution that rearranges patch-level gradient information to extract features from

similar regions while maintaining overall structure perception. Additionally, a dual-path HOG-guided self-attention mechanism captures global and local dependencies by reorganizing pixel-level gradient data for diverse degradation modeling. Before the final  $1 \times 1$  pointwise convolution, the reordered features are mapped back to their original spatial positions for consistency.

**Local Dynamic-range Convolution (LDRConv).** Traditional convolutions offer fixed receptive fields. This characteristic limits their compatibility with self-attention mechanisms, which excel at modeling long-range dependencies. To address this limitation, we propose a local dynamic-range convolution that reorganizes input features at the patch level using gradient magnitude and orientation prior to convolution. Specifically, given an input feature  $F \in \mathbb{R}^{C \times H \times W}$ , we first split it into  $F_1$  and  $F_2$ , and then sort  $F_1$  at the patch level and modulate it with bin-wise gradient features. The processed  $F_1$  is concatenated with  $F_2$ , and the result is passed through depth-wise convolution as follows:

$$\begin{aligned} F_1, F_2 &= \text{Split}(F), \quad F_1 = \text{Sort}_{\text{patch}}(F_1) + \text{HOG}(F_1), \\ F &= \text{Conv}_{3 \times 3}^d(\text{Conv}_{1 \times 1}^p(\text{Concat}(F_1, F_2))), \end{aligned} \quad (2)$$

where  $\text{Conv}_{1 \times 1}^p$  denotes  $1 \times 1$  point-wise convolution,  $\text{Conv}_{3 \times 3}^d$  denotes  $3 \times 3$  depth-wise convolution,  $\text{Sort}_{\text{patch}}(F_1)$  is the patch-level sorting based on gradient magnitude and orientation using

$$\begin{aligned} g_x &= S_x(F_1), \quad g_y = S_y(F_1), \\ m &= \sqrt{g_x^2 + g_y^2}, \quad o = \left\lfloor \frac{\text{atan2}(g_y, g_x) + \pi}{2\pi} N_{\text{bin}} \right\rfloor, \\ \mathbf{idx} &= \text{Sort}\left(\mathcal{R}_{C \times H \times W}^{N_{\text{patch}} \times C \times \frac{HW}{N_{\text{patch}}}}(o \cdot m)\right), \\ F_1 &= \mathcal{R}_{N_{\text{patch}} \times C \times \frac{HW}{N_{\text{patch}}}}^{C \times H \times W} \left( \text{Gather}\left(\mathcal{R}_{C \times H \times W}^{N_{\text{patch}} \times C \times \frac{HW}{N_{\text{patch}}}}(F_1), \mathbf{idx}\right) \right), \end{aligned} \quad (3)$$

and  $\text{HOG}(F_1)$  denotes the HOG features extraction, calculated as

$$\begin{aligned} \sum_i^{N_{\text{bin}}} H_{F_1}^{(N_{\text{patch}}, i)} &= \frac{1}{C \times HW / N_{\text{patch}}} m \cdot \delta(o = i), \\ \text{HOG}(F_1) &= \text{Conv}_{1 \times 1} \left( \mathcal{R}_{HW \times N_{\text{bin}}}^{N_{\text{bin}} \times H \times W} (\text{Up}_{N_{\text{patch}} \times N_{\text{bin}}}^{HW \times N_{\text{bin}}}(H_{F_1})) \right), \end{aligned} \quad (4)$$

where  $N_{\text{bin}}$  denotes the number of bins,  $\delta$  represents an indicator function. LDRConv can aggregate information from similar spatial positions without destroying the overall structure. The visualization results can be found in the supplementary materials.

**HOG Self-Attention.** Existing Vision Transformers [7, 50, 57, 70] typically adopt fixed spatial attention windows or restrict attention to channel-wise operations to reduce computational and memory cost. However, these rigid designs hinder the self-attention module from modeling long-range dependencies, which are important for reliable feature interactions. We observe that the same degradation usually leads to similar HOG response patterns. Pixels with background textures or varying degradation strength benefit from adaptive attention weighting. Therefore, we propose a HOG-guided attention module that categorizes spatial pixels into bins based on the HOG descriptor, and applies varying levels of attention across and within bins following [55].

Upon obtaining the output of LDRConv, we decompose it into a value feature  $V \in \mathbb{R}^{C \times H \times W}$  and two query-key pair sets  $F_{QK,1}$

and  $F_{QK,2} \in \mathbb{R}^{2C \times H \times W}$ , which are processed separately in distinct branches. We apply the HOG descriptor to classify spatial pixels into bins based on their HOG features. This classification aids in dynamically adjusting the attention weights, emphasizing areas with significant degradation or texture variations. The entire process is described in detail below:

$$\begin{aligned} \mathbf{idx} &= \text{Sort}\left(\mathcal{R}_{C \times H \times W}^{C \times HW}(o(V) \cdot m(V))\right), \\ V &= \text{Split}\left(\text{Gather}\left(\mathcal{R}_{C \times H \times W}^{C \times HW}(V), \mathbf{idx}\right)\right), \\ Q_1, K_1 &= \text{Split}\left(\text{Gather}\left(\mathcal{R}_{C \times H \times W}^{C \times HW}(F_{QK,1}), \mathbf{idx}\right)\right), \\ Q_2, K_2 &= \text{Split}\left(\text{Gather}\left(\mathcal{R}_{C \times H \times W}^{C \times HW}(F_{QK,2}), \mathbf{idx}\right)\right), \end{aligned} \quad (5)$$

where  $\mathcal{R}_{C \times H \times W}^{C \times HW}$  performs the reshaping of features from  $\mathbb{R}^{C \times H \times W}$  to  $\mathbb{R}^{C \times HW}$ ,  $\mathbf{idx}$  represents the sorted index, and the Gather operation extracts tensor elements using the given index. By specifying the number of bins  $B$ , we transform the sorted features in  $C \times HW$  into a tensor with dimensions  $C \times B \times (HW/B)$ . To capture both global and local information, we introduce two reshaping techniques: bin-wise histogram reshaping (BHOGR) and frequency-wise histogram reshaping (FHOGR). In BHOGR, we designate  $B$  bins, each holding  $HW/B$  elements; in FHOGR, we set the frequency per bin to  $B$ , resulting in  $HW/B$  bins. Thus, BHOGR aggregates many dispersed pixels to extract large-scale features, whereas FHOGR clusters pixels with similar intensity to capture fine-grained details. Subsequently, we process the two query-key sets through their respective reshaping and self-attention modules and merge their outputs element-wise to generate the final result as follows:

$$\begin{aligned} \mathbf{A}_B &= \text{softmax}\left(\frac{\mathcal{R}_B(Q_1)\mathcal{R}_B(K_1)^\top}{\sqrt{k}}\right) \mathbf{R}_B(V), \\ \mathbf{A}_F &= \text{softmax}\left(\frac{\mathcal{R}_F(Q_2)\mathcal{R}_F(K_2)^\top}{\sqrt{k}}\right) \mathbf{R}_F(V), \\ \mathbf{A} &= \mathbf{A}_B \otimes \mathbf{A}_F. \end{aligned} \quad (6)$$

Here,  $k$  is the number of heads,  $\mathcal{R}_{i \in \{B, F\}}$  represents the reshaping operation (BHOGR or FHOGR), and  $\mathbf{A}_i$  is the attention map.

### 3.3 Dynamic Interaction Feed-Forward

To enhance the adaptability of feed-forward layers to various degradation scenarios, we introduce a Dynamic Interaction Feed-Forward (DIFF) layer. For an input tensor  $F_l \in \mathbb{R}^{C \times H \times W}$ , we first apply pointwise convolution to expand the channel dimension by a factor of  $r$ . The expanded features then undergo pixel shuffling and channel shuffling before being split into two parallel branches. Each branch processes features differently: one uses  $5 \times 5$  depth-wise convolution, while the other employs dilated  $3 \times 3$  depth-wise convolution (dilation rate=2) to capture multi-scale information. Following [13, 55], we use a gating mechanism where the Mish-activated output from the second branch modulates the first branch. The fused features then undergo channel aggregation [28] to preserve crucial global

information. The complete process is formulated as follows:

$$\begin{aligned}
F_l^{\text{shuffled}} &= \text{ChannelShuffle}(\text{PixelShuffle}(\text{Conv}_{1 \times 1}(F_l)), 2), \\
F_{l,1}, F_{l,2} &= \text{Split}(F_l^{\text{shuffled}}), \\
F_{l,1} &= \text{Conv}_{5 \times 5}^d(F_{l,1}), \quad F_{l,2} = \text{Conv}_{3 \times 3}^{\text{d,dilated}}(F_{l,2}), \\
F_l^{\text{fused}} &= \text{Mish}(F_{l,2}) \odot F_{l,1}, \\
F_l^C &= F_l^{\text{fused}} + \gamma_c \left( F_l^{\text{fused}} - \text{GELU}(\text{Conv}_{1 \times 1}(F_l^{\text{fused}})) \right), \\
F_{l+1} &= \text{Conv}_{1 \times 1}(\text{PixelUnshuffle}(F_l^C)),
\end{aligned} \tag{7}$$

where  $\text{Conv}_{5 \times 5}^d$  represents  $5 \times 5$  depth-wise convolution,  $\text{PixelShuffle}$  and  $\text{PixelUnshuffle}$  represent pixel-shuffling and unshuffling operations,  $\text{Conv}_{3 \times 3}^{\text{d,dilated}=2}$  is  $3 \times 3$  dilated depth-wise convolution with dilation rate 2,  $\text{ChannelShuffle}$  represents the channel shuffling operation with 2 groups,  $\text{Mish}$  denotes the Mish activation [43],  $\text{GELU}$  is the Gaussian Error Linear Unit activation,  $\gamma_c$  represents the learnable element-wise scaling operation, and  $F_{l+1}$  is the output of current stage passing to  $(l+1)_{th}$  stage.

### 3.4 Loss Supervision

The reconstruction loss is defined as the  $L_1$  norm of the pixel-wise difference between the restored high-quality image  $\hat{I}^{hq}$  and the ground truth  $I^{gt}$ :

$$\mathcal{L}_{rec} = \|\hat{I}^{hq} - I^{gt}\|_1. \tag{8}$$

However,  $\mathcal{L}_{rec}$  regulates only pixel-level similarity. To overcome this limitation, we introduce two supplementary loss terms. To preserve the inherent intensity relationships in images, we define correlation loss [55] to regulate the linear relationship between the restored image and ground truth:

$$\mathcal{L}_{cor} = \frac{1}{2} (1 - \rho(\hat{I}^{hq}, I^{gt})), \tag{9}$$

where  $\rho(\hat{I}^{hq}, I^{gt})$  denotes the Pearson correlation coefficient between the restored and ground truth images. To enhance the structural and textural fidelity of restored images, we incorporate a differentiable HOG loss:

$$\mathcal{L}_{hog} = \|\text{HOG}(\hat{I}^{hq}) - \text{HOG}(I^{gt})\|_2^2, \tag{10}$$

where  $\text{HOG}(\cdot)$  denotes our differentiable HOG feature extraction layer. More details can be found in the supplemental material. This loss captures gradient orientation statistics in local image regions, effectively preserving important edge and texture information that pixel-wise losses may overlook. The overall loss function is defined as:

$$\mathcal{L} = \mathcal{L}_{rec} + \alpha \mathcal{L}_{cor} + \beta \mathcal{L}_{hog}, \tag{11}$$

where  $\alpha$  and  $\beta$  are the weights for balancing loss terms.

## 4 Experiments

### 4.1 Experimental Setup

To comprehensively evaluate our method, we perform experiments in two all-in-one image restoration settings based on prior work: (I) 3-task adverse weather removal [55], which includes desnowing, draining&dehazing, and raindrop removal. (II) 5-task image restoration [79], which includes deraining, low-light enhancement,

desnowing, dehazing, and deblurring. We train one model for each setting to handle various degradations.

**Datasets and Metrics.** For setting (I), we train and evaluate our method using the AllWeather [47, 55] dataset. For setting (II), we train and evaluate our method on five degradation-specific datasets: the merged dataset [19, 64] for deraining, LOL [65] for low-light enhancement, Snow100K [35] for desnowing, RESIDE [25] for dehazing, and GoPro [46] for deblurring. To further evaluate generalization capability, we evaluate HOGformer on real-world datasets: Practical [67] for deraining, MEF [42], NPE [59], and DICM [23] for low-light enhancement, HIDE [53] and RealBlur-J/R [52] for deblurring, and T-OLED [80] for under-display camera restoration. For evaluation metrics, we employ PSNR and SSIM for distortion measurement, and LPIPS [76] for perceptual quality assessment. In benchmark tests without reference images, we utilize NIQE [44], LOE [59], and IL-NIQE [75] as no-reference metrics.

### 4.2 Implementation Details.

We implement our model using PyTorch and conduct experiments on NVIDIA Tesla A100 GPUs. We apply random horizontal and vertical flips for data augmentation. Following Histoformer [55],  $\alpha$  is set to 1, and B equals the number of attention heads.  $N_{bin}$  is set to 9 according to original HOG setting [12].

**Setting (I).** The network is trained for 300,000 iterations with a batch size of 8 and patch size of 128, following the progressive learning approach in [55]. We use AdamW optimizer [38] with an initial learning rate of  $3e^{-4}$  for the first 92,000 iterations, then decrease it to  $1e^{-6}$  using cosine annealing [37] for the remaining 208,000 iterations. The number of blocks at each stage  $L_{i \in \{1,2,3,4\}}$  is set to  $\{4, 4, 6, 8\}$  with channel size  $C = 36$ . The DIFF module uses a channel expansion factor  $r = 2.667$ . Self-attention heads across the four stages are set to  $\{1, 2, 4, 8\}$  respectively.

**Setting (II).** The network is trained for 75,000 iterations using the AdamW optimizer with a learning rate of  $3e^{-4}$  and a batch size of 40. Each batch includes images for different tasks in the following proportions: dehazing (0.4), deraining (0.2), desnowing (0.2), low-light (0.1), and deblurring (0.1). Network inputs are randomly cropped to  $168 \times 168$  patches from original images. For the small version of HOGformer, each stage has 2 blocks ( $L_{i \in \{1,2,3,4\}}$ ) with a channel size of 24. The DIFF module and self-attention heads remain unchanged from Setting (I). The large version of HOGformer uses the same model as Setting (I).

### 4.3 Comparison with State-of-the-Arts

Table 1 compares the proposed method with task-specific and all-in-one state-of-the-art (SOTA) approaches across synthetic and real-world adverse weather datasets. For a fair comparison, we incorporate leading degradation removal methods (e.g., MPRNet [71], MAXIM [56], and Restormer [70]) as baselines. All-in-one models are retrained using AllWeather datasets [27, 47, 57] like HOGformer. Experimental results demonstrate that HOGformer outperforms existing methods, including GridFormer [61] and Histoformer [55], across all weather conditions, achieving substantial improvements in quantitative metrics. For qualitative comparison, as shown in Figures 3 and Figure 4, our method restores original colors and details, yielding more stable results. Additionally, as shown in Figure 5, our

**Table 1: Quantitative comparisons of three weather removal tasks using PSNR and SSIM. The top half of the tables shows results from task-specific methods, while the bottom half displays evaluations of all-in-one image restoration models. The best and second-best results are highlighted in red and blue. Methods marked with \* do not have available source codes.**

	Image Desnowing				Deraining & Dehazing				Raindrop Removal			
	Snow100K-S [35]		Snow100K-L [35]		Outdoor-Rain [26]		RainDrop [49]		Average			
	PSNR ↑	SSIM ↑	PSNR ↑	SSIM ↑	PSNR ↑	SSIM ↑	PSNR ↑	SSIM ↑	PSNR ↑	SSIM ↑		
SPANet [60]	29.92	0.8260	23.70	0.7930	CycleGAN [81]	17.62	0.6560	pix2pix [17]	28.02	0.8547	-	-
JSTASR [8]	31.40	0.9012	25.32	0.8076	pix2pix [17]	19.09	0.7100	DuRN [20]	31.24	0.9259	-	-
RESCAN [29]	31.51	0.9032	26.08	0.8108	HRGAN [26]	21.56	0.8550	RaindropAttn [51]	31.44	0.9263	-	-
SnowGAN [67]	32.33	0.9500	27.17	0.8983	PCNet [30]	26.19	0.9015	AttentiveGAN [49]	31.59	0.9274	-	-
DDMSNet [74]	34.34	0.9445	28.85	0.8772	MPRNet [71]	28.03	0.9192	IDT [51]	31.87	0.9313	-	-
DTANet [5]	34.79	0.9497	30.06	0.9017	NAFNet [7]	29.59	0.9027	MAXIM [56]	31.87	0.9352	-	-
Restormer [70]	36.01	0.9579	30.36	0.9068	Restormer [70]	30.03	0.9215	Restormer [70]	32.18	0.9408	-	-
All-in-One [27]*	-	-	28.33	0.8820	All-in-One [27]*	24.71	0.8980	All-in-One [27]*	31.12	0.9268	-	-
TransWeather [57]	32.51	0.9341	29.31	0.8879	TransWeather [57]	28.83	0.9000	TransWeather [57]	30.41	0.9157	30.27	0.9094
Chen et al. [9]	34.42	0.9469	30.22	0.9071	Chen et al. [9]	29.27	0.9147	Chen et al. [9]	31.81	0.9309	31.43	0.9249
WGWSNet [82]	34.31	0.9460	30.16	0.9007	WGWSNet [82]	29.32	0.9207	WGWSNet [82]	32.38	0.9378	31.54	0.9263
WeatherDiff <sub>64</sub> [47]	35.83	0.9566	30.09	0.9041	WeatherDiff <sub>64</sub> [47]	29.64	0.9312	WeatherDiff <sub>64</sub> [47]	30.71	0.9312	31.57	0.9308
WeatherDiff <sub>128</sub> [47]	35.02	0.9516	29.58	0.8941	WeatherDiff <sub>128</sub> [47]	29.72	0.9216	WeatherDiff <sub>128</sub> [47]	29.66	0.9225	30.99	0.9225
AWRCP [68]	36.92	0.9652	31.92	<b>0.9344</b>	AWRCP [68]	31.39	0.9329	AWRCP [68]	31.93	0.9314	33.04	0.9409
GridFormer [61]	37.46	0.9640	31.71	0.9231	GridFormer [61]	31.87	0.9335	GridFormer [61]	32.39	0.9362	33.36	0.9392
Histoformer [55]	<b>37.41</b>	<b>0.9656</b>	<b>32.16</b>	0.9261	Histoformer [55]	<b>32.08</b>	<b>0.9389</b>	Histoformer [55]	<b>33.06</b>	<b>0.9441</b>	<b>33.67</b>	<b>0.9436</b>
<b>HOGformer (Ours)</b>	<b>37.93</b>	<b>0.9685</b>	<b>32.41</b>	<b>0.9297</b>	<b>HOGformer (Ours)</b>	<b>32.89</b>	<b>0.9460</b>	<b>HOGformer (Ours)</b>	<b>32.72</b>	<b>0.9452</b>	<b>33.99</b>	<b>0.9474</b>

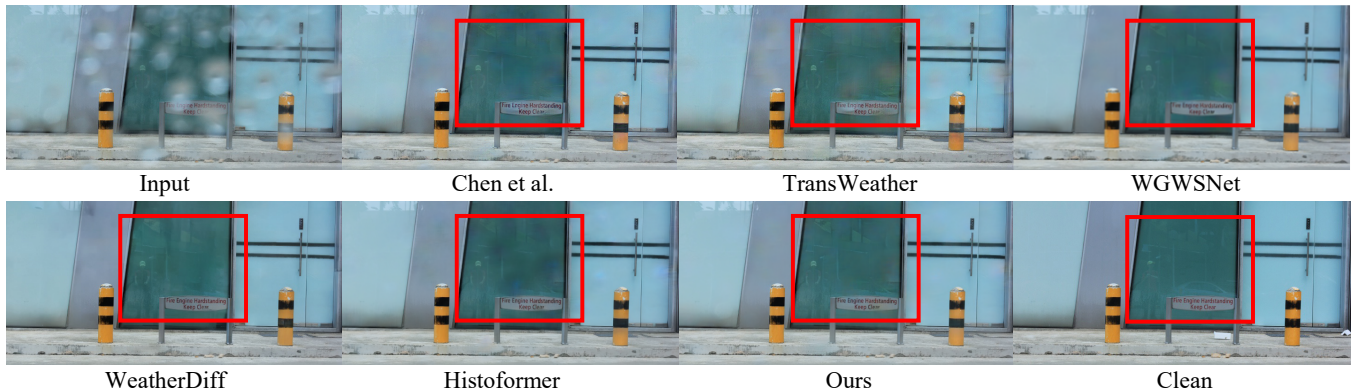


**Figure 3: Visual comparison for raindrop removal on RainDrop [49]. Zoom in for the best visualization.**

method effectively handles hybrid-weather degradation of rain, fog, and snow that has not been seen in training, while Histoformer fails, highlighting the superior generalization of our approach.

**Setting (II).** Table 2 provides a quantitative comparison of all-in-one image restoration methods across five natural degradations. HOGformer achieves an optimal balance between performance and complexity, outperforming both task-specific and general-purpose methods. HOGformer-S (2.91M parameters) excels in low-light enhancement (25.36dB PSNR, 0.915 SSIM), desnowing (32.72dB PSNR, 0.929 SSIM), and dehazing (33.67dB PSNR, 0.991 SSIM), while maintaining competitiveness in deraining and deblurring. HOGformer-S outperforms larger models such as DiffUIR-L (36.26M) and DA-CLIP (174.1M) in several metrics. HOGformer-L (16.64M parameters) achieves state-of-the-art performance across all tasks with far fewer parameters than DiffUIR-L (36.26M), Restormer (26.12M),

RDDM (36.26M), Prompt-IR (35.59M), and DA-CLIP (174.1M). Despite a higher computational cost (91.77G FLOPs), HOGformer-L is more efficient than heavier models like Painter and ProRes (248.9G). These results highlight the superior all-in-one restoration capabilities and efficiency of HOGformer. Qualitative results can be found in the supplementary materials.

To further assess the generalization of HOGformer, we conduct experiments on both seen and unseen image restoration tasks. In Table 3, HOGformer surpasses task-specific and all-in-one methods in deraining, enhancement, desnowing, and deblurring. Despite strong performance from prior SOTA methods like RDDM and Restormer, HOGformer maintains high perceptual quality across all evaluations. In Table 4, on the challenging T-OLED dataset with unseen degradations, HOGformer achieves comparable performance with SOTA methods. These results validate the effectiveness of HOGformer in addressing seen and unseen degradations.

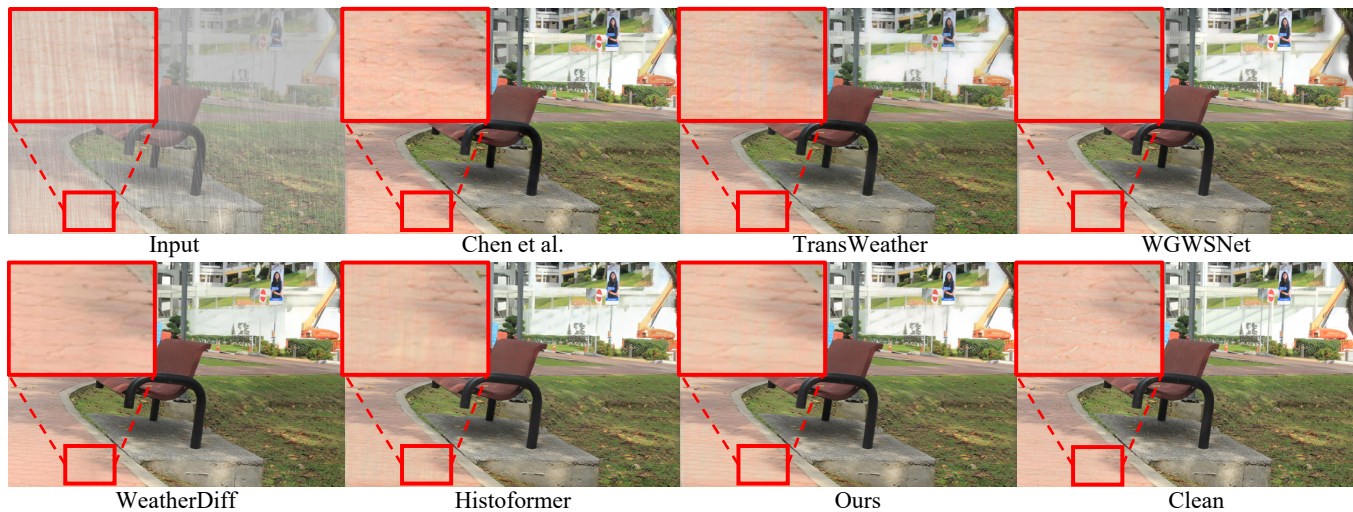


Figure 4: Visual comparison for deraining on Outdoor-Rain [26]. Zoom in for the best visualization.

Table 2: Quantitative results of all-in-one image restoration methods in five tasks. The best and second-best results are highlighted in red and blue. The top is task-specific restoration methods, and the bottom is all-in-one restoration methods.

	Deraining (5 sets)		Enhancement		Desnowing (2 sets)		Dehazing		Deblurring		Complexity	
	PSNR $\uparrow$	SSIM $\uparrow$	PSNR $\uparrow$	SSIM $\uparrow$	PSNR $\uparrow$	SSIM $\uparrow$	PSNR $\uparrow$	SSIM $\uparrow$	PSNR $\uparrow$	SSIM $\uparrow$	Params (M)	FLOPS (G)
SwinIR [31]	30.78	0.923	17.81	0.723	-	-	21.5	0.891	24.52	0.773	0.9	752.13
MIRNet-v2 [72]	<b>33.89</b>	0.924	<b>24.74</b>	0.851	-	-	24.03	0.927	26.30	0.799	5.9	140.92
DehazeFormer [54]	-	-	-	-	-	-	<b>34.29</b>	<b>0.983</b>	-	-	<b>4.63</b>	<b>48.64</b>
Restormer [70]	<b>33.96</b>	<b>0.935</b>	20.41	0.806	-	-	30.87	0.969	<b>32.92</b>	<b>0.961</b>	26.12	141
MAXIM [56]	33.24	<b>0.933</b>	<b>23.43</b>	<b>0.863</b>	-	-	<b>34.19</b>	<b>0.985</b>	<b>32.86</b>	<b>0.940</b>	14.1	216
DRSFormer [10]	33.15	0.927	-	-	-	-	-	-	-	-	33.7	242.9
IR-SDE [39]	-	-	-	-	20.45	0.787	-	-	30.70	0.901	34.2	98.3
WeatherDiff [47]	-	-	-	-	<b>33.51</b>	<b>0.939</b>	-	-	-	-	82.96	-
RDDM [34]	30.74	0.903	23.22	<b>0.899</b>	<b>32.55</b>	<b>0.927</b>	30.78	0.953	29.53	0.876	36.26	<b>9.88</b>
Restormer [70]	27.10	0.843	17.63	0.542	28.61	0.876	22.79	0.706	26.36	0.814	26.12	141
AirNet [24]	24.87	0.773	14.83	0.767	27.63	0.860	25.47	0.923	26.92	0.811	8.93	30.13
Painter [62]	29.49	0.868	22.40	0.872	-	-	-	-	-	-	307	248.9
IDR [73]	29.32	0.880	21.34	0.826	-	-	25.24	0.943	27.87	0.846	15.34	-
ProRes [41]	30.67	0.891	22.73	0.877	-	-	32.02	0.952	27.53	0.851	307	248.9
Prompt-IR [48]	29.56	0.888	22.89	0.847	-	-	32.02	0.952	27.21	0.817	35.59	15.81
DA-CLIP [40]	28.96	0.853	24.17	0.882	30.80	0.888	31.39	0.983	25.39	0.805	174.1	118.5
DiffUIR-S [79]	30.25	0.893	23.52	0.895	31.45	0.915	31.83	0.954	27.79	0.830	<b>3.27</b>	<b>2.40</b>
DiffUIR-L [79]	<b>31.03</b>	<b>0.904</b>	25.12	0.907	32.65	0.927	32.94	0.956	<b>29.17</b>	<b>0.864</b>	36.26	<b>9.88</b>
<b>HOGformer-S (Ours)</b>	30.75	0.901	<b>25.36</b>	<b>0.915</b>	<b>32.72</b>	<b>0.929</b>	<b>33.67</b>	<b>0.991</b>	28.37	0.840	<b>2.91</b>	20.63
<b>HOGformer-L (Ours)</b>	<b>31.63</b>	<b>0.914</b>	<b>25.57</b>	<b>0.917</b>	<b>34.08</b>	<b>0.941</b>	<b>36.60</b>	<b>0.994</b>	<b>29.95</b>	<b>0.884</b>	16.64	91.77

#### 4.4 Ablation Studies

In this section, we first conduct an ablation study to evaluate the contribution of the proposed core components on Outdoor-Rain [26]. Then, we explore the optimal hyperparameters of the proposed local dynamic-range convolution and HOG loss.

**Effectiveness of Core Components.** As illustrated in Table 5, the baseline model without any of our proposed modules serves as a reference point for comparison. Upon integrating the LDR-Conv module, we observe a notable improvement in both PSNR and SSIM metrics, demonstrating its effectiveness in enhancing feature representation. Further incorporating the DHOGSA mechanism yields additional performance gains, validating its capability

to capture gradient-sensitive attributes crucial for image restoration tasks. The introduction of the DIFF component further elevates the reconstruction quality by refining the feature transformation process. Finally, when all components are combined and trained with our proposed HOG Loss, the model achieves optimal performance, with significant improvements in both PSNR and SSIM compared to the baseline. These results comprehensively demonstrate that each proposed component makes a meaningful contribution to the overall performance, with their synergistic integration ultimately delivering state-of-the-art results for our task.

**Hyperparameters of Local Dynamic-range Convolution.** Figure 6 (a) illustrates the influence of patch size on the performance



Figure 5: Visual comparisons on hybrid-weather degradations. Zoom in for the best visualization.

Table 3: Quantitative results of known task generalization setting. The best and second-best results are highlighted in red and blue. The top is task-specific restoration methods, and the bottom is all-in-one restoration methods.

Method	Deraining		Enhancement		Desnowing		Deblurring	
	NIQE ↓	LOE ↓	NIQE ↓	LOE ↓	NIQE ↓	IL-NIQE ↓	PSNR ↑	SSIM ↑
WeatherDiff [47]	-	-	-	-	2.96	21.97	-	-
CLIP-LIT [33]	-	-	3.70	232.48	-	-	-	-
RDDM [34]	3.34	41.80	3.57	202.18	2.76	22.26	30.74	0.894
Restormer [64]	3.50	30.32	3.80	351.61	-	-	32.12	0.926
AirNet [24]	3.55	145.3	3.45	598.13	2.75	21.63	16.78	0.628
Prompt-IR [48]	3.52	28.53	3.31	255.13	2.79	23.00	22.48	0.770
DA-CLIP [40]	3.42	42.03	3.56	218.27	2.72	21.49	17.51	0.667
DiffUIR [79]	3.38	24.82	3.14	193.40	2.74	22.42	30.63	0.890
HOGformer (Ours)	3.31	26.45	3.08	112.12	2.69	21.77	30.92	0.907

Table 4: Quantitative results of unknown tasks setting on T-OLED [80]. The best and second-best results are highlighted in red and blue. The top is task-specific restoration methods, and the bottom is all-in-one restoration methods.

Method	T-OLED [80]		
	PSNR ↑	SSIM ↑	LPIPS ↓
NAFNet [5]	26.89	0.774	0.346
MPRNet [71]	23.33	0.807	0.383
DGUNet [45]	19.67	0.627	0.570
MIRNetV2 [72]	20.15	0.703	0.474
SwinIR [31]	17.72	0.661	0.519
RDDM [34]	17.00	0.626	0.545
Restormer [70]	20.98	0.632	0.360
DL [14]	21.23	0.656	0.434
Transweather [57]	20.52	0.666	0.451
AirNet [24]	22.73	0.739	0.374
IDR [73]	27.91	0.793	0.346
Prompt-IR [48]	20.47	0.669	0.462
DA-CLIP [40]	15.74	0.606	0.472
DiffUIR [79]	29.55	0.887	0.281
HOGformer (Ours)	29.33	0.889	0.271

of LDRConv. The baseline convolution yields 32.21dB PSNR and 0.9393 SSIM. Employing LDRConv with a patch size of 2 results in similar outcomes (32.24dB PSNR, 0.9392 SSIM), indicating that limited context hinders dynamic range adaptation. Increasing the patch size to 4 enhances performance (32.70dB PSNR, 0.9440 SSIM), while a patch size of 8 delivers the best performance (32.89dB PSNR,

Table 5: Ablation study on the contribution of the proposed core components.

LDRConv	DHOGSA	DIFF	HOG Loss	PSNR↑	SSIM↑
×	×	×	×	30.14	0.9258
✓	×	×	×	30.49	0.9261
✓	✓	×	×	31.68	0.9358
✓	✓	✓	×	32.40	0.9421
✓	✓	✓	✓	32.89	0.9460

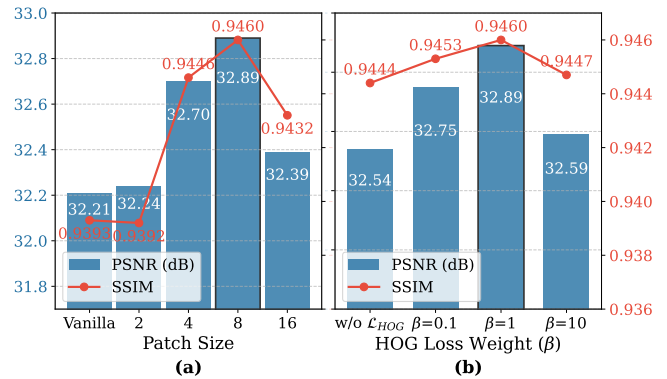


Figure 6: Ablation studies on the patch size of local dynamic-range convolution (a) and the weight of HOG loss (b).

0.9460 SSIM), surpassing the baseline by 0.68dB PSNR and 0.0067 SSIM. However, using a patch size of 16 leads to reduced performance, likely due to excessive context and incomplete structural preservation. These results indicate that a patch size of 8 represents the optimal balance between contextual information and structural retention.

#### Hyperparameters of HOG Loss.

Figure 6 (b) demonstrates the effect of the weighting parameter  $\beta$  on the proposed HOG loss. For  $\beta = 0$ , the baseline performance is 32.54dB PSNR and 0.9444 SSIM. Introducing a small weight ( $\beta = 0.1$ ) increases the performance to 32.75dB PSNR and 0.9453 SSIM, highlighting the benefit of incorporating gradient information. The optimal results occur at  $\beta = 1$ , yielding 32.89dB PSNR and 0.9460 SSIM, reflecting a substantial improvement over the baseline (+0.35dB PSNR, +0.0016 SSIM). However, a larger weight ( $\beta = 10$ ) reduces performance, suggesting that an overemphasis on gradients may compromise overall reconstruction quality. These results indicate that  $\beta = 1$  is the optimal hyperparameter.

## 5 Discussion and Conclusion

In this paper, we present HOGformer, an all-in-one image restoration model that leverages the power of Histogram of Oriented Gradients (HOG) features. Through a Dynamic HOG-aware Self-Attention (DHOGSA) mechanism and innovative network components, HOGformer effectively handles diverse image degradations. Our approach demonstrates state-of-the-art performance while maintaining computational efficiency. Future research directions include exploring HOG-based mechanisms in conjunction



with emerging architectures (e.g., Mamba) to address the all-in-one restoration task.

Additionally, although the proposed framework advances all-in-one degradation handling, there is still room for enhancing the generalization to unseen or more complex degradation scenarios. Generalization to novel degradation patterns persists as a fundamental challenge in all-in-one restoration frameworks. Potential solutions may involve developing robust training paradigms, including adversarial learning and meta-learning strategies, to enhance adaptation to unforeseen degradations.

## Acknowledgments

This work was supported by the National Natural Science Foundation of China under Grant U24A20251, Shenzhen Science and Technology Program under Grant JCYJ20230807111107015, Fundamental Research Funds for the Central Universities, Sun Yat-sen University under Grant 24lgqb015.

## References

- Yuang Ai, Huaibo Huang, and Ran He. 2024. LoRA-IR: Taming Low-Rank Experts for Efficient All-in-One Image Restoration. *arXiv preprint arXiv:2410.15385* (2024).
- Yuang Ai, Huaibo Huang, Xiaoqiang Zhou, Jiexiang Wang, and Ran He. 2024. Multimodal prompt perceiver: Empower adaptiveness generalizability and fidelity for all-in-one image restoration. In *Proceedings of the IEEE/CVF Conference on Computer Vision and Pattern Recognition*. 25432–25444.
- Mark R Banham and Aggelos K Katsaggelos. 1997. Digital image restoration. *IEEE signal processing magazine* 14, 2 (1997), 24–41.
- Yuanhao Cai, Hao Bian, Jing Lin, Haoqiang Wang, Radu Timofte, and Yulun Zhang. 2023. Retinexformer: One-stage retinex-based transformer for low-light image enhancement. In *Proceedings of the IEEE/CVF international conference on computer vision*. 12504–12513.
- Liangyu Chen, Xiaojie Chu, Xiangyu Zhang, and Jian Sun. 2022. Simple baselines for image restoration. In *European conference on computer vision*. Springer, 17–33.
- Li Chen, Penghao Wu, Kashyap Chitta, Bernhard Jaeger, Andreas Geiger, and Hongyang Li. 2024. End-to-end autonomous driving: Challenges and frontiers. *IEEE Transactions on Pattern Analysis and Machine Intelligence* (2024).
- Sixiang Chen, Tian Ye, Yun Liu, Erkang Chen, Jun Shi, and Jingchun Zhou. 2022. Snowformer: Scale-aware transformer via context interaction for single image desnowing. *arXiv preprint arXiv:2208.09703* 2 (2022).
- Wei-Ting Chen, Hao-Yu Fang, Jian-Jiun Ding, Cheng-Che Tsai, and Sy-Yen Kuo. 2020. JSTASR: Joint size and transparency-aware snow removal algorithm based on modified partial convolution and veiling effect removal. In *Computer Vision—ECCV 2020: 16th European Conference, Glasgow, UK, August 23–28, 2020, Proceedings, Part XXI* 16. Springer, 754–770.
- Wei-Ting Chen, Zhi-Kai Huang, Cheng-Che Tsai, Hao-Hsiang Yang, Jian-Jiun Ding, and Sy-Yen Kuo. 2022. Learning multiple adverse weather removal via two-stage knowledge learning and multi-contrastive regularization: Toward a unified model. In *Proceedings of the IEEE/CVF conference on computer vision and pattern recognition*. 17653–17662.
- Xiang Chen, Hao Li, Mingqiang Li, and Jinshan Pan. 2023. Learning a sparse transformer network for effective image deraining. In *Proceedings of the IEEE/CVF Conference on Computer Vision and Pattern Recognition*. 5896–5905.
- Marcos V Conde, Gregor Geigle, and Radu Timofte. 2024. Instructir: High-quality image restoration following human instructions. In *European Conference on Computer Vision*. Springer, 1–21.
- Navneet Dalal and Bill Triggs. 2005. Histograms of oriented gradients for human detection. In *2005 IEEE computer society conference on computer vision and pattern recognition (CVPR'05)*, Vol. 1. Ieee, 886–893.
- Yann N Dauphin, Angela Fan, Michael Auli, and David Grangier. 2017. Language modeling with gated convolutional networks. In *International conference on machine learning*. PMLR, 933–941.
- Qingnan Fan, Dongdong Chen, Lu Yuan, Gang Hua, Nenghai Yu, and Baoquan Chen. 2019. A general decoupled learning framework for parameterized image operators. *IEEE transactions on pattern analysis and machine intelligence* 43, 1 (2019), 33–47.
- Hang Guo, Jinmin Li, Tao Dai, Zhihao Ouyang, Xudong Ren, and Shu-Tao Xia. 2024. Mambair: A simple baseline for image restoration with state-space model. In *European conference on computer vision*. Springer, 222–241.
- Zongyao He and Zhi Jin. 2024. Latent modulated function for computational optimal continuous image representation. In *Proceedings of the IEEE/CVF Conference on Computer Vision and Pattern Recognition*. 26026–26035.
- Phillip Isola, Jun-Yan Zhu, Tinghui Zhou, and Alexei A Efros. 2017. Image-to-image translation with conditional adversarial networks. In *Proceedings of the IEEE conference on computer vision and pattern recognition*. 1125–1134.
- Junjun Jiang, Zengyuan Zuo, Gang Wu, Kui Jiang, and Xianming Liu. 2024. A survey on all-in-one image restoration: Taxonomy, evaluation and future trends. *arXiv preprint arXiv:2410.15067* (2024).
- Kui Jiang, Zhongyuan Wang, Peng Yi, Chen Chen, Baojin Huang, Yimin Luo, Jiayi Ma, and Junjun Jiang. 2020. Multi-scale progressive fusion network for single image deraining. In *Proceedings of the IEEE/CVF conference on computer vision and pattern recognition*. 8346–8355.
- Kui Jiang, Zhongyuan Wang, Peng Yi, Chen Chen, Zheng Wang, Xiao Wang, Junjun Jiang, and Chia-Wen Lin. 2021. Rain-free and residue hand-in-hand: A progressive coupled network for real-time image deraining. *IEEE Transactions on Image Processing* 30 (2021), 7404–7418.
- Yitong Jiang, Zhaoyang Zhang, Tianfan Xue, and Jinwei Gu. 2024. Autodir: Automatic all-in-one image restoration with latent diffusion. In *European Conference on Computer Vision*. Springer, 340–359.
- Lingshun Kong, Jiangxin Dong, Jianjun Ge, Mingqiang Li, and Jinshan Pan. 2023. Efficient frequency domain-based transformers for high-quality image deblurring. In *Proceedings of the IEEE/CVF Conference on Computer Vision and Pattern Recognition*. 5886–5895.
- Chulwoo Lee, Chul Lee, and Chang-Su Kim. 2013. Contrast enhancement based on layered difference representation of 2D histograms. *IEEE transactions on image processing* 22, 12 (2013), 5372–5384.
- Boyun Li, Xiao Liu, Peng Hu, Zhongqin Wu, Jiancheng Lv, and Xi Peng. 2022. All-in-one image restoration for unknown corruption. In *Proceedings of the IEEE/CVF conference on computer vision and pattern recognition*. 17452–17462.
- Boyi Li, Wenqi Ren, Dengpan Fu, Dacheng Tao, Dan Feng, Wenjun Zeng, and Zhangyang Wang. 2018. Benchmarking single-image dehazing and beyond. *IEEE Transactions on Image Processing* 28, 1 (2018), 492–505.
- Ruoteng Li, Loong-Fah Cheong, and Robby T Tan. 2019. Heavy rain image restoration: Integrating physics model and conditional adversarial learning. In *Proceedings of the IEEE/CVF conference on computer vision and pattern recognition*. 1633–1642.
- Ruoteng Li, Robby T Tan, and Loong-Fah Cheong. 2020. All in one bad weather removal using architectural search. In *Proceedings of the IEEE/CVF conference on computer vision and pattern recognition*. 3175–3185.
- Siyuan Li, Zedong Wang, Zicheng Liu, Cheng Tan, Haitao Lin, Di Wu, Zhiyuan Chen, Jiangbin Zheng, and Stan Z Li. 2024. MogaNet: Multi-order Gated Aggregation Network. In *ICLR*.
- Xia Li, Jianlong Wu, Zhouchen Lin, Hong Liu, and Hongbin Zha. 2018. Recurrent squeeze-and-excitation context aggregation net for single image deraining. In *Proceedings of the European conference on computer vision (ECCV)*. 254–269.
- Yu Li, Robby T Tan, Xiaojie Guo, Jiabing Lu, and Michael S Brown. 2016. Rain streak removal using layer priors. In *Proceedings of the IEEE conference on computer vision and pattern recognition*. 2736–2744.
- Jingyun Liang, Jiezhong Cao, Guolei Sun, Kai Zhang, Luc Van Gool, and Radu Timofte. 2021. Swinir: Image restoration using swin transformer. In *Proceedings of the IEEE/CVF international conference on computer vision*. 1833–1844.
- Pengwei Liang, Junjun Jiang, Xianming Liu, and Jiayi Ma. 2024. Image deblurring by exploring in-depth properties of transformer. *IEEE Transactions on Neural Networks and Learning Systems* (2024).
- Zhexin Liang, Chongyi Li, Shangchen Zhou, Ruicheng Feng, and Chen Change Loy. 2023. Iterative prompt learning for unsupervised backlit image enhancement. In *Proceedings of the IEEE/CVF International Conference on Computer Vision*. 8094–8103.
- Jiawei Liu, Qiang Wang, Huijie Fan, Yinong Wang, Yandong Tang, and Liangqiong Qu. 2024. Residual denoising diffusion models. In *Proceedings of the IEEE/CVF Conference on Computer Vision and Pattern Recognition*. 2773–2783.
- Yun-Fu Liu, Da-Wei Jaw, Shih-Chia Huang, and Jenq-Neng Hwang. 2018. Desnownet: Context-aware deep network for snow removal. *IEEE Transactions on Image Processing* 27, 6 (2018), 3064–3073.
- Ze Liu, Yutong Lin, Yue Cao, Han Hu, Yixuan Wei, Zheng Zhang, Stephen Lin, and Baining Guo. 2021. Swin transformer: Hierarchical vision transformer using shifted windows. In *Proceedings of the IEEE/CVF international conference on computer vision*. 10012–10022.
- Ilya Loshchilov and Frank Hutter. 2016. Sgdr: Stochastic gradient descent with warm restarts. *arXiv preprint arXiv:1608.03983* (2016).
- Ilya Loshchilov, Frank Hutter, et al. 2017. Fixing weight decay regularization in adam. *arXiv preprint arXiv:1711.05101* 5 (2017), 5.
- Ziwei Luo, Fredrik K Gustafsson, Zheng Zhao, Jens Sjölund, and Thomas B Schön. 2023. Image restoration with mean-reverting stochastic differential equations. *arXiv preprint arXiv:2301.11699* (2023).
- Ziwei Luo, Fredrik K Gustafsson, Zheng Zhao, Jens Sjölund, and Thomas B Schön. 2024. Controlling vision-language models for universal image restoration. In *International Conference on Learning Representations*.

- [41] Jiaqi Ma, Tianheng Cheng, Guoli Wang, Qian Zhang, Xinggong Wang, and Lefei Zhang. 2023. Prores: Exploring degradation-aware visual prompt for universal image restoration. *arXiv preprint arXiv:2306.13653* (2023).
- [42] Kede Ma, Kai Zeng, and Zhou Wang. 2015. Perceptual quality assessment for multi-exposure image fusion. *IEEE Transactions on Image Processing* 24, 11 (2015), 3345–3356.
- [43] Diganta Misra. 2019. Mish: A self regularized non-monotonic activation function. *arXiv preprint arXiv:1908.08681* (2019).
- [44] Anish Mittal, Rajiv Soundararajan, and Alan C Bovik. 2012. Making a “completely blind” image quality analyzer. *IEEE Signal processing letters* 20, 3 (2012), 209–212.
- [45] Chong Mou, Qian Wang, and Jian Zhang. 2022. Deep generalized unfolding networks for image restoration. In *Proceedings of the IEEE/CVF conference on computer vision and pattern recognition*. 17399–17410.
- [46] Seungjun Nah, Tae Hyun Kim, and Kyoung Mu Lee. 2017. Deep multi-scale convolutional neural network for dynamic scene deblurring. In *Proceedings of the IEEE conference on computer vision and pattern recognition*. 3883–3891.
- [47] Ozan Özenizci and Robert Legenstein. 2023. Restoring vision in adverse weather conditions with patch-based denoising diffusion models. *IEEE Transactions on Pattern Analysis and Machine Intelligence* 45, 8 (2023), 10346–10357.
- [48] Vaishnav Potlapalli, Syed Waqas Zamir, Salman H Khan, and Fahad Shahbaz Khan. 2023. Promptir: Prompting for all-in-one image restoration. *Advances in Neural Information Processing Systems* 36 (2023), 71275–71293.
- [49] Rui Qian, Robby T Tan, Wenhan Yang, Jiajun Su, and Jiaying Liu. 2018. Attentive generative adversarial network for raindrop removal from a single image. In *Proceedings of the IEEE conference on computer vision and pattern recognition*. 2482–2491.
- [50] Yuwei Qiu, Kaihao Zhang, Chenxi Wang, Wenhan Luo, Hongdong Li, and Zhi Jin. 2023. Mb-taylorformer: Multi-branch efficient transformer expanded by taylor formula for image dehazing. In *Proceedings of the IEEE/CVF International Conference on Computer Vision*. 12802–12813.
- [51] Ruijie Quan, Xin Yu, Yuanzhi Liang, and Yi Yang. 2021. Removing raindrops and rain streaks in one go. In *Proceedings of the IEEE/CVF conference on computer vision and pattern recognition*. 9147–9156.
- [52] Jaesung Kim, Haeyun Lee, Jucheol Won, and Sunghyun Cho. 2020. Real-world blur dataset for learning and benchmarking deblurring algorithms. In *Computer Vision—ECCV 2020: 16th European Conference, Glasgow, UK, August 23–28, 2020, Proceedings, Part XXV 16*. Springer, 184–201.
- [53] Ziyi Shen, Wenguan Wang, Xiankai Lu, Jianbing Shen, Haibin Ling, Tingfa Xu, and Ling Shao. 2019. Human-aware motion deblurring. In *Proceedings of the IEEE/CVF international conference on computer vision*. 5572–5581.
- [54] Yuda Song, Zhuqing He, Hui Qian, and Xin Du. 2023. Vision transformers for single image dehazing. *IEEE Transactions on Image Processing* 32 (2023), 1927–1941.
- [55] Shangquan Sun, Wenqi Ren, Xinwei Gao, Rui Wang, and Xiaochun Cao. 2024. Restoring images in adverse weather conditions via histogram transformer. In *European Conference on Computer Vision*. Springer, 111–129.
- [56] Zhengzhong Tu, Hossein Talebi, Han Zhang, Feng Yang, Peyman Milanfar, Alan Bovik, and Yinxiao Li. 2022. Maxim: Multi-axis mlp for image processing. In *Proceedings of the IEEE/CVF conference on computer vision and pattern recognition*. 5769–5780.
- [57] Jeya Maria Jose Valanarasu, Rajeev Yasarla, and Vishal M Patel. 2022. Transweather: Transformer-based restoration of images degraded by adverse weather conditions. In *Proceedings of the IEEE/CVF conference on computer vision and pattern recognition*. 2353–2363.
- [58] Chenxi Wang, Hongjun Wu, and Zhi Jin. 2023. Fourllie: Boosting low-light image enhancement by fourier frequency information. In *Proceedings of the 31st ACM International Conference on Multimedia*. 7459–7469.
- [59] Shuhang Wang, Jin Zheng, Hai-Miao Hu, and Bo Li. 2013. Naturalness preserved enhancement algorithm for non-uniform illumination images. *IEEE transactions on image processing* 22, 9 (2013), 3538–3548.
- [60] Tianyu Wang, Xin Yang, Ke Xu, Shaozhe Chen, Qiang Zhang, and Rynson WH Lau. 2019. Spatial attentive single-image deraining with a high quality real rain dataset. In *Proceedings of the IEEE/CVF conference on computer vision and pattern recognition*. 12270–12279.
- [61] Tao Wang, Kaihao Zhang, Ziqian Shao, Wenhan Luo, Bjorn Stenger, Tong Lu, Tae-Kyun Kim, Wei Liu, and Hongdong Li. 2024. Gridformer: Residual dense transformer with grid structure for image restoration in adverse weather conditions. *International Journal of Computer Vision* 132, 10 (2024), 4541–4563.
- [62] Xinlong Wang, Wen Wang, Yue Cao, Chunhua Shen, and Tiejun Huang. 2023. Images speak in images: A generalist painter for in-context visual learning. In *Proceedings of the IEEE/CVF Conference on Computer Vision and Pattern Recognition*. 6830–6839.
- [63] Zhendong Wang, Xiaodong Cun, Jianmin Bao, Wengang Zhou, Jianzhuang Liu, and Houqiang Li. 2022. Uformer: A general u-shaped transformer for image restoration. In *Proceedings of the IEEE/CVF conference on computer vision and pattern recognition*. 17683–17693.
- [64] Zhouxia Wang, Jiawei Zhang, Runjian Chen, Wenping Wang, and Ping Luo. 2022. Restoreformer: High-quality blind face restoration from ungraded key-value pairs. In *Proceedings of the IEEE/CVF conference on computer vision and pattern recognition*. 17512–17521.
- [65] Chen Wei, Wenjing Wang, Wenhan Yang, and Jiaying Liu. 2018. Deep retinex decomposition for low-light enhancement. *arXiv preprint arXiv:1808.04560* (2018).
- [66] Gang Wu, Junjun Jiang, Kui Jiang, and Xianming Liu. 2024. Harmony in diversity: Improving all-in-one image restoration via multi-task collaboration. In *Proceedings of the 32nd ACM International Conference on Multimedia*. 6015–6023.
- [67] Wenhan Yang, Robby T Tan, Jiashi Feng, Jiaying Liu, Zongming Guo, and Shuicheng Yan. 2017. Deep joint rain detection and removal from a single image. In *Proceedings of the IEEE conference on computer vision and pattern recognition*. 1357–1366.
- [68] Tian Ye, Sixiang Chen, Jinbin Bai, Jun Shi, Chenghao Xue, Jingxia Jiang, Junjie Yin, Erkang Chen, and Yun Liu. 2023. Adverse weather removal with codebook priors. In *Proceedings of the IEEE/CVF international conference on computer vision*. 12653–12664.
- [69] Eduard Zamfir, Zongwei Wu, Nancy Mehta, Yuedong Tan, Danda Pani Paudel, Yun-lun Zhang, and Radu Timofte. 2025. Complexity Experts are Task-Discriminative Learners for Any Image Restoration. In *CVPR*. Springer.
- [70] Syed Waqas Zamir, Aditya Arora, Salman Khan, Munawar Hayat, Fahad Shahbaz Khan, and Ming-Hsuan Yang. 2022. Restormer: Efficient transformer for high-resolution image restoration. In *Proceedings of the IEEE/CVF conference on computer vision and pattern recognition*. 5728–5739.
- [71] Syed Waqas Zamir, Aditya Arora, Salman Khan, Munawar Hayat, Fahad Shahbaz Khan, Ming-Hsuan Yang, and Ling Shao. 2021. Multi-stage progressive image restoration. In *Proceedings of the IEEE/CVF conference on computer vision and pattern recognition*. 14821–14831.
- [72] Syed Waqas Zamir, Aditya Arora, Salman Khan, Munawar Hayat, Fahad Shahbaz Khan, Ming-Hsuan Yang, and Ling Shao. 2022. Learning enriched features for fast image restoration and enhancement. *IEEE transactions on pattern analysis and machine intelligence* 45, 2 (2022), 1934–1948.
- [73] Jinghao Zhang, Jie Huang, Mingde Yao, Zizheng Yang, Hu Yu, Man Zhou, and Feng Zhao. 2023. Ingredient-oriented multi-degradation learning for image restoration. In *Proceedings of the IEEE/CVF Conference on Computer Vision and Pattern Recognition*. 5825–5835.
- [74] Kaihao Zhang, Rongqing Li, Yanjiang Yu, Wenhan Luo, and Changsheng Li. 2021. Deep dense multi-scale network for snow removal using semantic and depth priors. *IEEE Transactions on Image Processing* 30 (2021), 7419–7431.
- [75] Lin Zhang, Lei Zhang, and Alan C Bovik. 2015. A feature-enriched completely blind image quality evaluator. *IEEE Transactions on Image Processing* 24, 8 (2015), 2579–2591.
- [76] Richard Zhang, Phillip Isola, Alexei A Efros, Eli Shechtman, and Oliver Wang. 2018. The unreasonable effectiveness of deep features as a perceptual metric. In *Proceedings of the IEEE conference on computer vision and pattern recognition*. 586–595.
- [77] Shansi Zhang, Nan Meng, and Edmund Y Lam. 2023. LRT: An efficient low-light restoration transformer for dark light field images. *IEEE Transactions on Image Processing* 32 (2023), 4314–4326.
- [78] Xiaozhe Zhang, Fengying Xie, Haidong Ding, Shaocheng Yan, and Zhenwei Shi. 2024. Proxy and Cross-Stripes Integration Transformer for Remote Sensing Image Dehazing. *IEEE Transactions on Geoscience and Remote Sensing* (2024).
- [79] Dian Zheng, Xiao-Ming Wu, Shuzhou Yang, Jian Zhang, Jian-Fang Hu, and Wei-Shi Zheng. 2024. Selective hourglass mapping for universal image restoration based on diffusion model. In *Proceedings of the IEEE/CVF Conference on Computer Vision and Pattern Recognition*. 25445–25455.
- [80] Yuqian Zhou, David Ren, Neil Emerton, Sehoon Lim, and Timothy Large. 2021. Image restoration for under-display camera. In *Proceedings of the IEEE/CVF conference on computer vision and pattern recognition*. 9179–9188.
- [81] Jun-Yan Zhu, Taesung Park, Phillip Isola, and Alexei A Efros. 2017. Unpaired image-to-image translation using cycle-consistent adversarial networks. In *Proceedings of the IEEE international conference on computer vision*. 2223–2232.
- [82] Yurui Zhu, Tianyu Wang, Xueyang Fu, Xuanyu Yang, Xin Guo, Jifeng Dai, Yu Qiao, and Xiaowei Hu. 2023. Learning weather-general and weather-specific features for image restoration under multiple adverse weather conditions. In *Proceedings of the IEEE/CVF conference on computer vision and pattern recognition*. 21747–21758.